Original Article

Institution of MECHANICAL ENGINEERS

Journal of RAIL AND RAPID TRANSIT

Proc IMechE Part F:
J Rail and Rapid Transit
2015, Vol. 229(8) 841–851

DOI: 10.1177/0954409714523583
pif.sagepub.com

SAGE

Parametric study of axle box acceleration at squats

Maria Molodova, Zili Li, Alfredo Núñez and Rolf Dollevoet

Abstract

This paper presents a study of the parameters that influence the detection of squats when using axle box acceleration (ABA) measurements. The analysed parameters include the train speed, the location of the squat in the track relative to the sleeper, and the track design. The study is conducted relying on a validated finite element model. The ABA measurements are found to be highly influenced by train speed. To model this influence, a practical method is proposed to represent the relationship between the train speed and relevant characteristics of ABA (magnitude and frequency) at a given squat. Such practical relationships provide the opportunity to map the ABA signals when it proves impossible to run measuring trains at a constant speed (as is the case with any in-service railway vehicle). The parameter study also indicates that the major frequency characteristics of ABA at squats are strongly related to the natural frequencies of the track. This conclusion is validated by performing hammer tests on the railway track. It is suggested that a proper characterization of the tracks will lead to a better understanding of the ABA signals. Finally, it is claimed that the results presented in this paper can be used as a guideline to calibrate or improve squat detection algorithms based on ABA measurements on a track.

Keywords

Axle box acceleration, squats, finite element model, short-wave track defects, dynamic simulations, frequency response function, vibrations of railway track, condition monitoring

Date received: 15 July 2013; accepted: 20 January 2014

Introduction

Short-wave anomalies in tracks, such as damaged frogs, damaged insulated joints, hanging sleepers and ballast voids, can cause increased-magnitude dynamic train/track forces that lead to degradation of the railway infrastructure. In particular, squats are special cases of short track defects that are characterized by local depressions of the contact surface of the rail accompanied by cracks[1], as shown in Figure 1.

Squats initiate at an indentation on the rail surface, at welds or on a corrugated track.[2–4] Impact contact forces on early-stage squats can lead to the development of cracks and accelerated degradation of track, whose timely prevention can reduce costs. In general, the maintenance costs of tracks are typically higher than other maintenance costs (e.g. costs of the wheels, other parts of the trains, catenaries); however, the renewal cost of a track is significantly high and can easily exceed the total operational cost. In particular, when squats are detected in their early stage, they can be treated by grinding a thin layer from the rail surface; this is significantly cheaper than the cost of a complete replacement of the track at a later and severe stage of degradation. For this reason, research on new methods to detect these anomalies in an early stage, when the maintenance costs are still comparatively low, is very important for the railway industry.

However, most of the track inspections that look for squats are currently performed manually, this means that the technicians visit the tracks or watch video recordings of tracks to perform a visual inspection. This type of inspection is effective for detecting problems at a late stage of degradation (because the problems can be easily observed) but is not scalable or practical when the monitoring of a very large railway network is required; it is very intensive for the workers and expensive in terms of the amount of man-hours needed to monitor the entire railway network. Additionally, manual inspection cannot identify early-stage squats because those anomalies are difficult to assess visually and because frequent updates of the railway track conditions are needed to observe

Faculty of Civil Engineering and Geosciences, Delft University of Technology, The Netherlands

Corresponding author:
Zili Li, Section of Road and Railway Engineering, Faculty of Civil Engineering and Geosciences, Delft University of Technology, Stevinweg 1, 2628 CN Delft, The Netherlands.
Email: Z.li@tudelft.nl

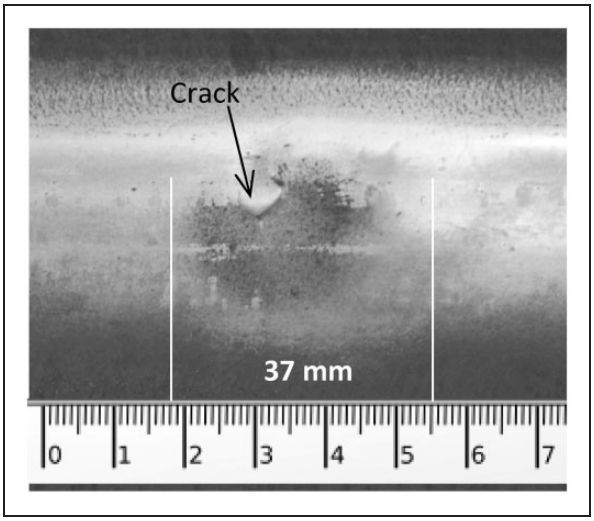

Figure 1. A squat.

their evolution. The use of on-train measurement systems based on accelerometers has been considered as an automatic and efficient monitoring system of the state of tracks. Previous research has shown that axle box acceleration (ABA) measurements can indicate short track defects, such as poor-quality insulated joints, corrugation and welds.[5–8] At the Delft University of Technology, Section of Road and Railway Engineering, new methods for the automatic and quick detection of squats employing ABA measurements are being developed and validated using real-life measurements on the Dutch railway network.[9] Molodova et al.[10] performed a feasibility study on detecting early-stage squats using ABA and found that squats could be detected by analysing the frequency content of the signals. Molodova et al.[11] and Molodova[12],using finite element (FE) modelling, determined that the frequencies related to squats (signature tunes) are 300 Hz and 1060–1160 Hz, with a brief high-frequency response of up to 2000 Hz. It was shown that the shape of the squat is an important parameter that modifies the magnitude of the signature tunes. Also, quantitative relationships between the geometrical characteristics of squats (i.e. length and depth) and the ABA signal were investigated.[11,12] However, the influence of various test conditions on the signature tunes of squats has not yet been studied. For example, validation measurements need to be obtained using specialized measurement trains under a controlled constant speed and conditions that are not typical for in-service railway vehicles.

This paper discusses some aspects that must be considered for the real-life implementation of any squat detection method based on ABA measurements. Although Spanner[13] has already found that ABA measurements are speed-dependent, the current study aims to determine what those dependencies are, and whether the use of real in-service trains to obtain reliable ABA measurements is possible. It has been observed in Li et al.[14] that squats appear more often near the sleepers; this suggests that it is necessary to analyse the extent to which the ABA responses differ when the squat is at different locations on the track in terms of both their frequency and time-domain responses. Regarding the physical components, the resonance frequencies of track vibrations are dependent on the stiffness and damping properties of the track. The ABA measurements are also dependent on these properties. Finally, by using numerical simulations, it is shown that the algorithm used to detect squats for each type of track can be improved by including additional information about the parameters.

The results of this paper rely on FE simulations. An FE model already validated by field measurements[10] is used in this paper. Track parameters were determined through field measurements using a sledgehammer. The track parameters used in this paper are those of the Dutch railways, but the approach is applicable to any track.

FE model

The effect of train speed on the signature tunes of squats, the influence of track parameters and the location of the squat relative to the sleeper on ABA are studied. FE modelling is used to establish quantitative relationships between squats and ABA characteristics under controlled parameter conditions. Dynamic simulations of the wheel rolling over a rail with a squat at various speeds are considered. Illustrations of the three-dimensional (3D) FE model are shown in Figure 2.

Symmetry considerations meant that only a half of the wheel-set and a half of the track, which is 10 m long, are required to be considered in the model. From field measurements it was observed that the frequencies excited at squats and interesting for detection are above 200 Hz. Thus, the FE model used in this study was validated with real measurements in the 200–2000 Hz frequency range. The model was not validated for the low-frequency range. For example, for the case of effects related to bending of the rail constrained between the wheels of a bogie, the distance between the wheels in the bogie of the measuring train was 2.5 m. The wavelength is therefore 2.5 m and the corresponding frequency is 12 Hz for a train speed of 30 m/s, so it is not important for the detection of squats. On the other hand, the two wheels could also cause pre-loading of the track for each other and could change the eigen frequencies. However, according to Zhao et al.[15] the static and dynamic wheel load is almost zero at three sleeper spaces, that is, at a distance of 1.8 m. As in general, the distance between two wheels of railway rolling stock is not less than 1.8 m, the cross- influence of the contact forces from two wheels will be insignificant.

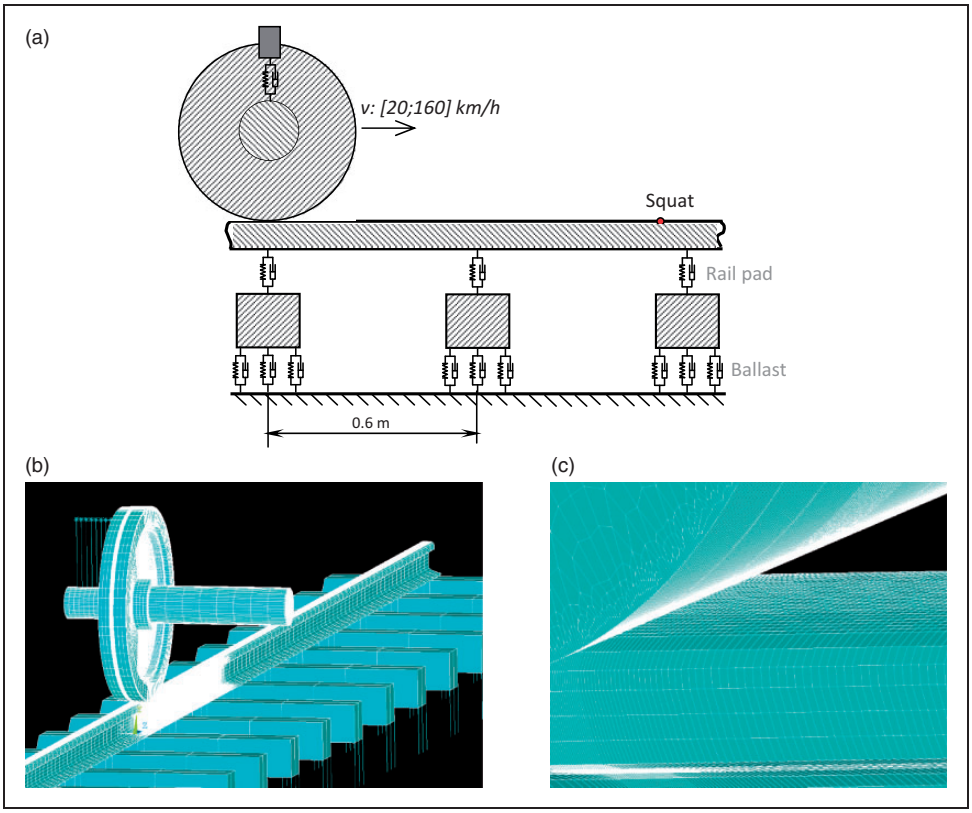

Figure 2. (a) Side view of the 3D FE model; (b) overview of the 3D FE model; (c) closed-up of the mesh in the contact area. The track model is 10 m long.

The vehicle load was modelled as a sprung mass. The half wheel-set, the rail and the sleepers were modelled with 3D solid elements, representing their real geometry and material properties. The material of the wheel and rail was taken to be elastic, with an elastic-plastic layer on the contact surfaces. The rail was 54E1 with a 1:40 inclination.[16] The rail pads and ballast were modelled as springs and dampers. The smallest element size on the contact surfaces was approximately 1.3 mm. The parameters of the model[17] were normal parameters observed from Dutch railway track and were abstracted from Hiensch et al.[17] (see Table 1).

A squat was modelled as a vertical deviation of the rail surface. The model was calibrated using real ABA measurements at artificial uniform cuts as shown in Figure 3. The vertical-longitudinal geometry of this defect is shown in Figure 3(a); in the lateral direction, the defect was modelled as uniform in terms of width and depth. Compared with real-shaped squats, a defect with a uniform shape in the lateral direction may cause increased dynamic excitation but this is not important for detection systems based on frequency content.[14,18] In practice, the main features of the frequency response of ABA at those defects was in good agreement with the ones obtained from ABA at real-shaped squats. Regarding cracks, they were not considered in this simulation because this research considers the early stage of the squat's development. The bottom of squats is always rusty, which means that there is no contact between the wheel and the rail surface at the deepest point of a squat. In the simulation, the wheel radius was 460 mm and the length of the part of the defect with no contact was 20 mm. Then, the depth of the squat should be greater

Table 1. Parameters of the model based on data from ref. [17].

Component	Parameter	Value
Track parameters		
Rail pad	Stiffness	1300 MN/m
	Damping	45 kNs/m
Sleeper	Mass	244 kg
	Sleeper distance	0.6 m
Ballast	Stiffness	45 MN/m
	Damping	32 kNs/m
Vehicle parameters		
Sprung mass	Mass	8000 kg
First suspension	Stiffness	1.15 MN/m
	Damping	2500 Ns/m
Wheel and rail		
Material	Young's modulus	210 GPa
	Poisson's ratio	0.3
	Mass density	7800 kg/m^3
	Yield stress	0.8 GPa
	Tangent modulus	21 GPa

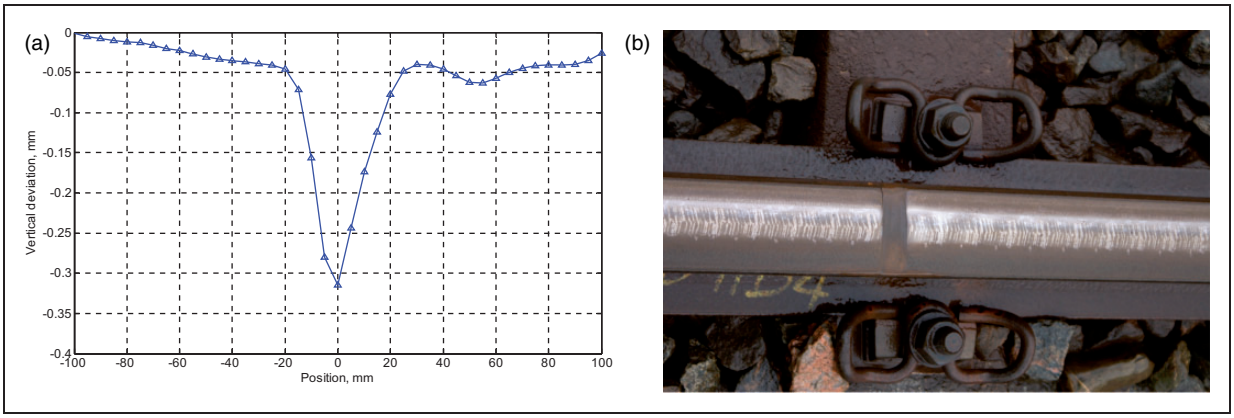

Figure 3. Modelled rail surface defect. The defect was uniform in terms of width and depth in the lateral direction (a) vertical-longitudinal profile and (b) artificial defect.

than 0.1 mm. On the other hand, based on measurements of many squats, their depth is usually less than 0.4 mm[19] and therefore a depth of 0.3 mm was chosen. Such an initial depth can be caused by a hard object trapped in the wheel/rail contact. The model of the squat was applied to the nominal rail surface by vertically shifting the surface nodes of the rail.

The running speed of the wheel was varied between 20 and 160 km/h. The numerical solution process was a combination of an implicit integration part, which calculates the static equilibrium and initial deformation of the wheel/track system, and an explicit integration part for dynamic simulation of the wheel rolling over the rail toward the squat.[12] Spanner[13] has stated that speed dependency is one of the limitations of ABA measurements. In this paper, the relation between ABA and train speed is investigated using numerical simulations based on an FE model. The use of a mapping to eliminate the influence of the train speed, if possible, is also discussed.

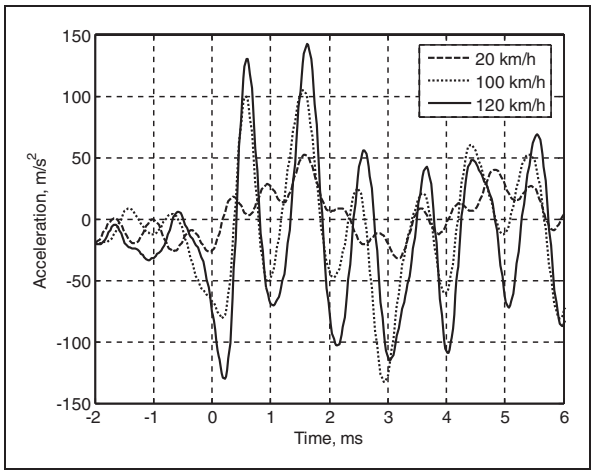

Figure 4. ABA values calculated at different speeds.

Variation of the train speed

Maximum ABA with different speeds

Figure 4 presents three of the ABA signals calculated around the squat. Because the wavelengths of ABA signals are dependent on the running speed, the ABA signals were compared in the time domain. Based on theoretical analysis and also field measurements, it was observed from the wavelength related to squats and ABA measurements that the frequency range related to squats is up to 2000 Hz for speed of 140 km/h.[14,18] The model was validated up to 2000 Hz using Matlab; the signals were filtered with a low-pass Butterworth filter with a cut-off frequency of 2000 Hz and shifted so that the maximum ABA peaks coincided.

The geometry of the surface defect (Figure 3(a)) applied on the rail surface in the model starts at −100 mm. In Figure 4, the variation in magnitude of the three curves before excitation is caused by the wheel moving on the rail, as the moving wheel causes vibration of the wheel/track system. The difference between the curves should be a result of the difference in speed of the moving loads. As can be observed in Figure 4, the vibration amplitude is larger for higher speeds. The waveform (shape of the response) was very similar in the time domain for train speeds between 80 and 160 km/h. The average wavelength (average distance between consecutive crests) was approximately 38 mm for a normal traffic speed of 140 km/h.

Figure 5 presents the relation between the maximum ABA values and train speed. These data were fitted with a third-order polynomial function

$$ABA_{\max} = 0.00009v^3 - 0.0273v^2 + 2.9679v + 1.2974, \quad v \in [20, 160]\ \text{km/h} \tag{1}$$

where v is the train speed (unit: km/h) and $ABA_{\max}$ is the maximum ABA (unit: m/s^2). The root-mean-squared error of the polynomial fit was 5.8 m/s^2.

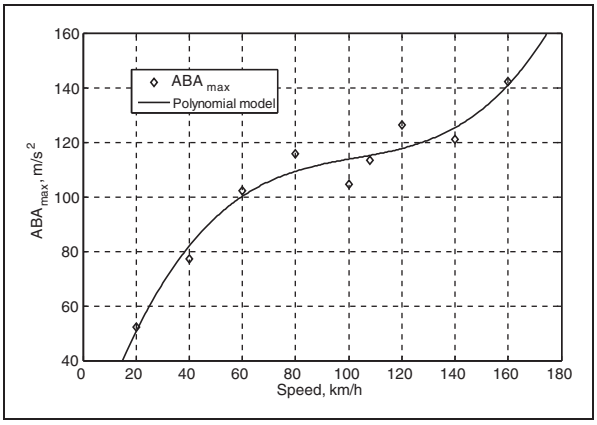

Figure 5. Relation between the maximum ABA and train speed.

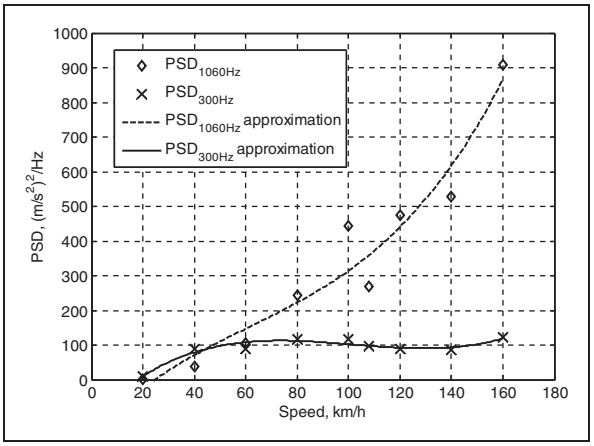

Figure 6. Relation between the PSD of acceleration and the train speed. Diamonds and crosses are calculated by FE simulations.

Power spectrum density of ABA with variation of train speed

A previous investigation indicated that the two major characteristic frequencies of ABA at squats were approximately 300 and 1060 Hz.[11,12] They are related to resonances of the vehicle/track system. In this section, the influence of the train speed on the power of the major frequencies is investigated. For practical squat detection applications, the power spectrum density (PSD) of the broader frequency band can be defined as follows

$$PSD_{300\mathrm{Hz}} = \max_{200<f<400}\{PSD(f)\} \tag{2}$$

$$PSD_{1060\mathrm{Hz}} = \max_{1000<f<1200}\{PSD(f)\} \tag{3}$$

where f is the frequency. In this paper, the PSD was calculated for the ABA signal, including the impact and subsequent vibration response. The signal used to calculate the PSD was 500 mm long, consisting in 100 mm before the impact and 400 mm after the impact.

Figure 6 illustrates that the power of the first major characteristic frequency ($PSD_{300\mathrm{Hz}}$) changes only slightly with the train speed. The relation between $PSD_{300\mathrm{Hz}}$ and the train speed can be approximated with a third-order polynomial function

$$PSD_{300\mathrm{Hz}} = 0.0003v^3 - 0.0796v^2 + 7.4472v - 108.66,\quad v \in [20,\ 160]\ \mathrm{km/h} \tag{4}$$

The power of the second major characteristic frequency $PSD_{1060\mathrm{Hz}}$ is highly dependent on the train speed. The relation between $PSD_{1060\mathrm{Hz}}$ and the train speed can be approximated with a second-order polynomial function

$$PSD_{1060\,\mathrm{Hz}} = 0.0328v^2 - 0.0071v - 4.4725,\quad v \in [20,\ 160]\ \mathrm{km/h} \tag{5}$$

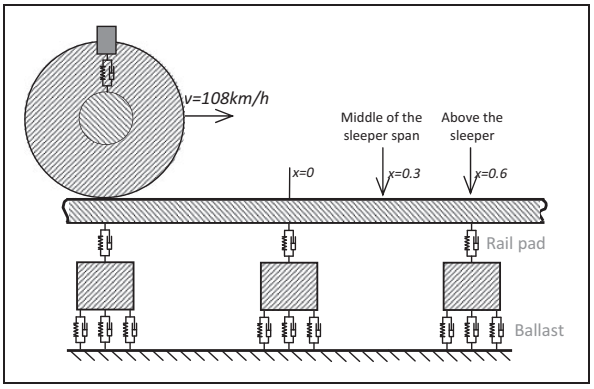

Figure 7. Illustration of the 3D FE model.

The equations (1), (4) and (5) were obtained only for one squat. The variation of the severity of squats must be investigated further to develop a mapping between the ABA characteristics and train speed.

Variation of the location of a squat

Li et al.[14] have stated that in practice most squats are found near the sleepers. Next, as shown in Figure 7, the relation between the squat location and ABA signals is investigated. Different cases are used to illustrate the difference: a squat located in the middle of the sleeper span, a squat located above the sleeper, and 14 other squats in different locations. The FE model was generally the same as in the previous section, and the wheel speed was 108 km/h (the typical speed of certain track sections in the Netherlands). The geometry of the simulated squat was the same as in Figure 3.

The maximum ABA for the above the sleeper case was approximately 20% higher than that for the in the middle of the sleeper span case (Figure 8). The wavelength of the ABA is also dependent on the location of

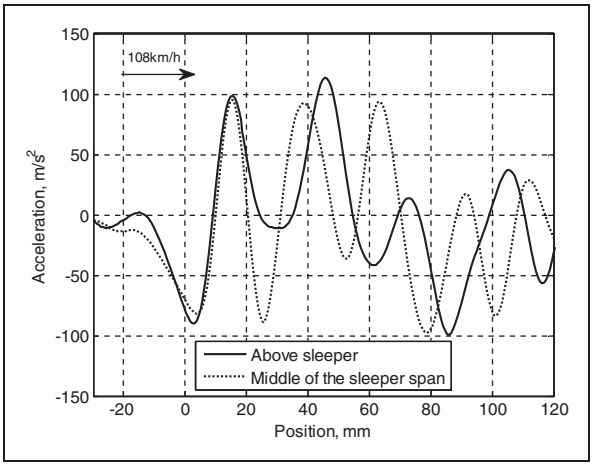

Figure 8. ABA signal at a squat located in the middle of the sleeper span and above the sleeper.

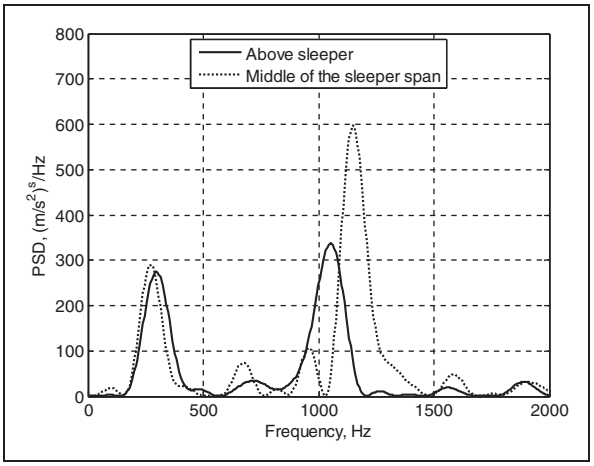

Figure 9. PSD of ABA signal at a squat located in the middle of the sleeper span and above the sleeper.

the squat relative to the sleeper and was varied from 24 mm for a squat located above the sleeper to 30 mm for a squat located in the middle of the sleeper span.

Figure 9 illustrates that the first characteristic frequency, 300 Hz, is relatively constant and does not depend on the squat location; the second characteristic frequency component changes its value from 1060 Hz, for the squat located above the sleeper, to 1160 Hz, for the squat located in the middle of the sleeper span.

Figure 10(a) and (b) presents the wavelet power spectrum (WPS) of the calculated cases. The red areas around the abscissa zero indicate the squat. For a squat located in the middle of the sleeper span (Figure 10(a)), the high energy response appears at approximately 1200 Hz; after 150 mm, when the wheel approaches the next sleeper, the frequency drops to 1000 Hz; the average frequency is approximately 1160 Hz. The response for the squat located above the sleeper appears at 1060 Hz (Figure 10(b)).

The relation between the maximum ABA and squat location can be approximated with a fourth-order polynomial function

$$ABA_{\max} = 4471.7x^4 - 9413.1x^3 + 6701.4x^2 - 1843.8x + 256.26, \quad x \in [0.3, 0.9]\text{m} \tag{6}$$

where $x = 0.3$ and $x = 0.9$ are in the middle of the sleeper span and $x = 0.6$ is above the sleeper, as shown in Figure 11. Relations between the powers of the major two ABA characteristics are shown in Figure 12. These relations can be approximated as follows (general trends)

$$PSD_{1060\,\text{Hz}} = -22,162x^4 + 62,239x^3 - 58,968x^2 + 22,004x - 2233.8, \quad x \in [0.3, 0.9]\text{m} \tag{7}$$

$$PSD_{300\,\text{Hz}} = 13,841x^4 - 32,212x^3 + 27,008x^2 - 9642.8x + 1502.8, \quad x \in [0.3, 0.9]\text{m} \tag{8}$$

Variation of the track parameters

Molodova et al.[11] and Molodova[12] have stated that the major frequencies observed in ABA measurements at squats are identical for squats of different severities, with the only difference being in the values of the power around those frequencies. This section investigates whether those frequencies are related with the natural frequencies of the vehicle/track system. Even if the measurements are performed on the same vehicle, the signature tunes of the squats might be dependent on the natural frequencies of the track, which vary at different track structures. Then, the natural frequencies of the track system are studied, and the signature tunes of the squats are revised.

Frequency response function

A frequency response function or transfer function expresses the structural response to an applied force as a function of vibration frequencies. The response may be given in terms of displacement, velocity or acceleration. The transfer function that describes the response of the structure in terms of displacement is called the receptance, and the transfer function that describes the response in terms of acceleration is called the inertance. The transfer functions help to determine the resonant frequencies of the track.

A technique called harmonic analysis was employed to calculate the receptance. This technique can predict the dynamic behaviour of a structure by estimating the steady state response of a linear

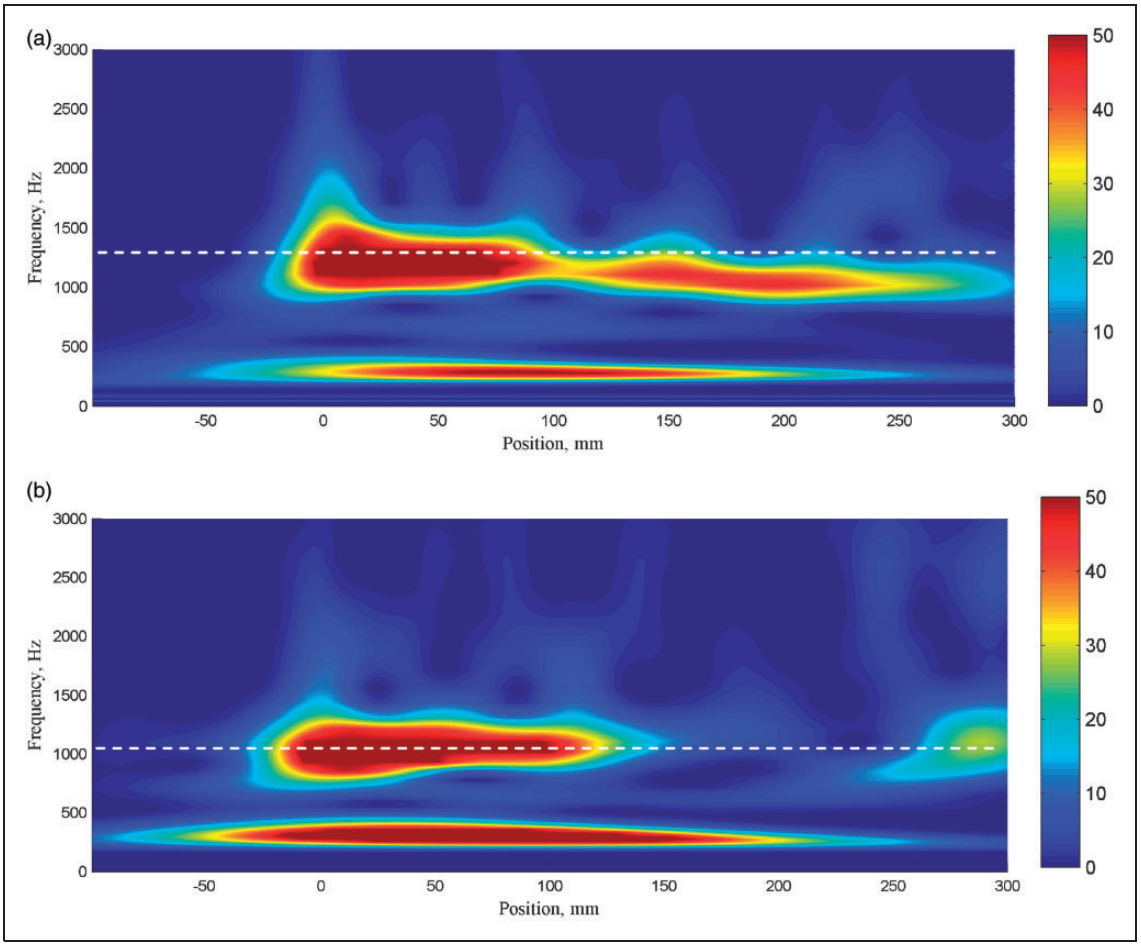

Figure 10. WPS of the normalized ABA at squats with different positions relative to the sleeper (a) mid-span position of a squat and (b) position of a squat above the sleeper. The signals are aligned so that position 0 is at the deepest point of the squat.

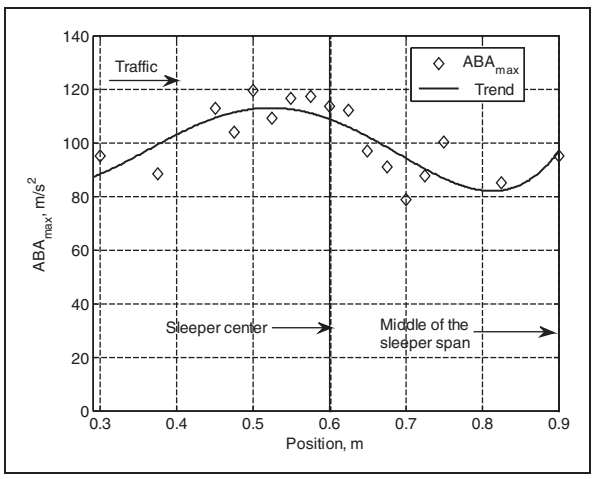

Figure 11. Relation between the maximum ABA and squat location.

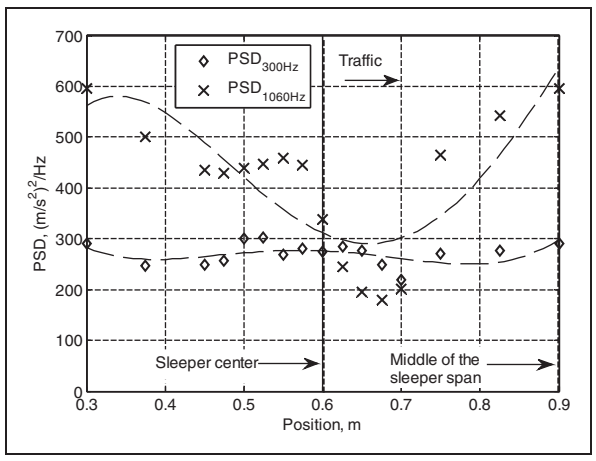

Figure 12. Relation between the acceleration PSD and squat location.

structure to loads that vary harmonically with time. The track receptance was estimated with the FE model, including the rail and its support. The setup of this experiment is shown in Figure 13.

The length of the simulated track was set to 20 m to minimize the effect of wave reflection from rail ends. The reduction of the track length to 10 m (as in previous sections), lead to about 15 to 20% differences in the calculated magnitudes of ABA, but no significant variation in the frequency characteristic was observed for track lengths of 10, 20 and 40 m. The track parameters were the same as in the previous simulations. A load of 20 N, varying harmonically in the frequency

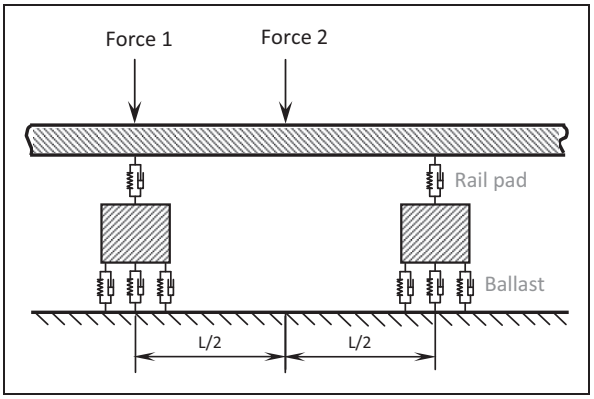

Figure 13. Configuration for harmonic analysis. The track is 20 m long.

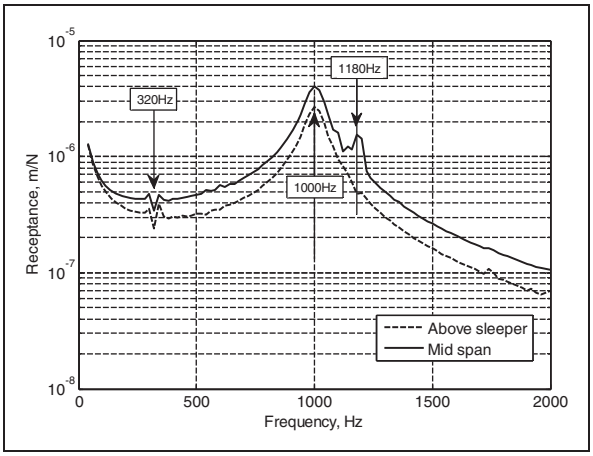

Figure 14. Receptance by FE harmonic analysis.

range 100–2000 Hz, was applied to the rail. Two simulations were performed: with the load (Force 1) applied above the sleeper and with the load (Force 2) in the mid-span, as shown in Figure 13. The load was applied far from the rail ends to avoid numerical problems.

The classification of the rail vertical modes has been previously presented in a number of papers in the literature.[8,20,21] The vertical vibration modes of a ballasted track are as follows.

1. Full track resonance, which is also called the in-phase vibration mode, is the vertical vibration of the rail moving together with the sleepers.
2. Sleeper anti-resonance is a vibration mode when the rail exhibits hardly any movement while the sleepers experience resonance.
3. Rail resonance, which is also called the out-of-phase vibration mode, is a vibration of the rail relative to the support; it corresponds to the opposite vibration of the rail and sleepers. The rail vertical resonance lies in the mid- or high-frequency range depending on the rail pad parameters.
4. Pin-pin resonance is a vibration of the rail with a wavelength of twice the sleeper spacing, with the rails pinned at the sleepers. The pin-pin resonance occurs in the high-frequency range. Pin-pin resonance is a vibration mode that appears at a fundamental mode and several higher modes.[22]

The receptance function calculated by harmonic response analysis is shown in Figure 14. The receptance displays anti-resonance at 320 Hz, which should be the sleeper anti-resonance. The resonance observed at 1000 Hz should be the rail resonance. A modal analysis is presented below to confirm these vibration modes. The next resonance, which is the pin-pin resonance, is observed only in the mid-span at 1180 Hz, and on-support anti-resonance is observed at the same frequency. These results agree with the results presented by Grassie et al.[23], where it was shown that the frequency response of the track to a harmonic force varies as the point of application of the force moves through the sleeper span. There are another two resonances at 1740 and 1920 Hz.

Modes of vibration

Modal analysis was used to determine the modes of vibrations of the track corresponding to the previously estimated resonance frequencies. Two track models were estimated: a pre-loaded track, including the track and wheel (Figure 2), and an unloaded track, i.e. only the track.

The modes of the pre-loaded track were calculated in two steps. First, a static analysis was performed to calculate the stress state. Then, modal analysis was performed considering the effect of the stress. A limitation of the modal analysis is that any nonlinearity, such as contact, will be ignored. Therefore, the stiffness of the contact elements was calculated based on their initial status and did not change, this resulted in a larger penetration. The modes of the unloaded track were calculated only in the second step, this is a modal analysis in which the structure was assumed to be stress-free.

Figure 15(a) presents the full track resonance, when the rail vibrates with the sleepers. Full track resonance was observed at 90 Hz for the unloaded track. Figure 15(b) presents the sleeper anti-resonance. The red and blue colours indicate the maximum amplitudes of the vibration in the opposite directions. The vibration amplitudes of the sleepers are higher than those of the rail. The sleeper anti-resonance was observed at 307 Hz, which is in agreement with the 320 Hz obtained by harmonic response analysis. The rail resonance was observed at 1006 Hz, as shown in Figure 15(c). The rail and sleepers move in opposite directions at the rail resonance, as indicated by the colours in Figure 15(c): green when sleepers move downward and light green when sleepers move upward. The rail resonance frequency is in agreement with that obtained by harmonic response analysis. Figure 15(d) presents the pin-pin resonance with a wavelength of twice the sleeper spacing and

zero amplitude at the sleepers. The pin-pin resonance was observed at 1192 Hz.

The effect of the pre-load was significant only on the full track resonance, which was 38 Hz for the pre-loaded track; the differences for the remaining resonant frequencies of the pre-loaded track were less than 1.6% compared with the frequencies of unloaded track (see Table 2). The effect of the pre-load can be more significant in actual cases[24], although this behaviour was not observed in this model due to its linear nature.

Validation of the frequency response function

The results obtained by the FE time-domain simulation, FE harmonic analysis and modal analysis were validated by a hammer test performed on the track. The hammer test is an impact test where the impact load and track accelerations are measured to calculate the frequency response function. The impact load applied with a hammer was measured with a force sensor on the hammer. The response of the track structure was measured with accelerometers mounted close to the excitation points. The configuration for the hammer test was similar to that shown in Figure 13, with the excitation points above the sleeper and in the mid-span. The test locations were free from rail top defects, such as squats or corrugation.

The inertance calculated from the hammer test is presented in Figure 16. Full track resonance was observed at 100 Hz, sleeper anti-resonance was observed at 280 Hz, rail resonance was observed at 1008 Hz, and pin-pin resonance was observed at 1150 Hz. There are also a number of resonances in the higher frequency range, including 1360, 1580 and 1880 Hz.

The sleeper anti-resonance observed at 320 Hz in the calculated receptance is in agreement with the 280 Hz measured inertance. The rail resonance at 1000 Hz in the receptance is in agreement with the 1008 Hz measured inertance; and the pin-pin resonance at 1180 Hz in the receptance is in agreement with the 1150 Hz measured inertance. There are also a number of other resonances in the higher-frequency range in the measured inertance: 1360, 1580 and 1880 Hz. For the first two frequencies the

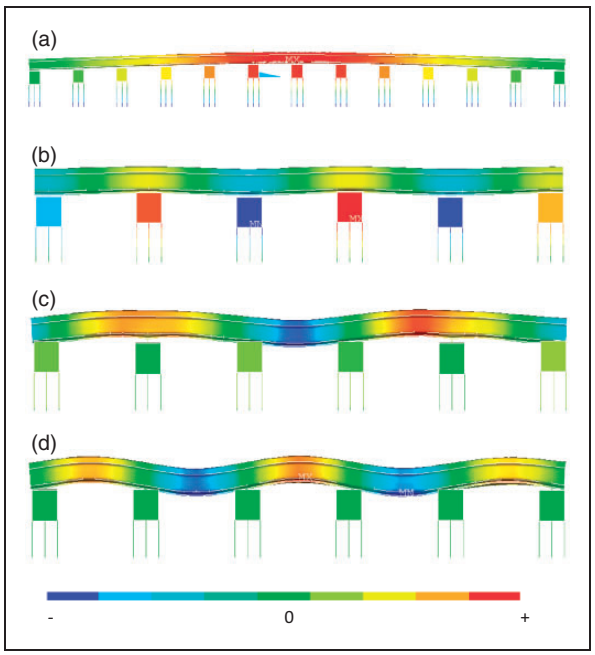

Figure 15. Track vibration modes: (a) full track resonance; (b) sleeper anti-resonance; (c) rail vertical mode; and (d) pin-pin resonance. The colours indicate the magnitude of the vibrations. (A color version of this figure is available in online).

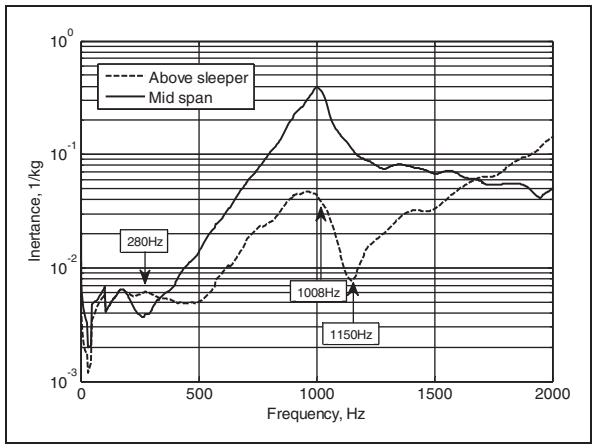

Figure 16. Inertance obtained using the hammer test on the track.

Table 2. Track resonant frequencies.

Signature tunes	Harmonic analysis	Stress-free modal analysis	Pre-stressed modal analysis	Hammer test	Resonance
–	–	90	38	100	Full track
300	320	307	308	280	Sleeper anti-resonance
1000	1000	1006	1012	1008	Rail vertical
1160	1180	1192	1211	1150	Pin-pin resonance
1530	–	1584	1587	1580	Rail vertical
1900	1920	1926	1926	1880	Rail vertical

counterparts are very weak in the calculated receptance, but the last frequency is in agreement with the 1920 Hz in the receptance. In the low frequencies (below 200 Hz) the model was not validated, so no correspondence can be seen with the measurement.

Relation between the signature tunes of squats and the track parameters

Table 2 summarizes the results obtained by FE simulations of ABA, harmonic analysis, modal analysis and the hammer test. The frequencies obtained by the different methods agree with each other. The differences between the results calculated with harmonic analysis and modal analysis are due to the resolution: the calculated receptance has only one point each 20 Hz (column 'Harmonic analysis' in Table 2). Small differences in resonant frequencies can result from the fact that the measured track may have already degraded, whereas the FE model uses the nominal track parameters. These differences are negligible. The presented FE model is capable of reproducing the track vibration frequencies in the range from 200 to 2000 Hz.

Comparing the signature tunes of the squats to track resonances, it becomes clear that the first major frequency component of the ABA measurement, approximately 300 Hz, is a sleeper anti-resonance. The second major frequency observed in the ABA signal when the squat is located around the sleeper, approximately 1000 Hz, is rail resonance. When the squat is located between the sleepers, the second major frequency of the ABA signal is approximately 1160 Hz, which is pin-pin resonance. The higher frequencies are rail vibration modes.

The signature tunes of squats are dependent on track parameters because they are the natural frequencies of the track. If the track is considered as a simple two-degree-of-freedom system (the rail and sleeper), the sleeper anti-resonance frequency is determined by the stiffness of the rail pads and ballast and the mass of the sleeper.[20] In reality, the sleeper anti-resonance frequency may also be dependent on the rail fastening system. The rail resonance is mainly dependent on the rail pad stiffness and rail mass.

The pin-pin resonance is mainly determined by the rail and is not affected by the track stiffness or sleepers. The pin-pin resonance can be estimated as the fundamental frequency of a simply supported beam of length L. If the Euler–Bernoulli beam theory is used, the pin-pin resonance can be estimated as follows[25]

$$f_{pp} = \frac{\pi}{2L^2}\sqrt{\frac{EI}{m_r}} \tag{9}$$

where EI is the bending stiffness of the rail, L is sleeper spacing, and m_r is mass of the rail per unit length.

Because the signature tunes of the squats are dependent on the track parameters, the detection algorithm should be adjusted for each track to improve its performance. Thus, the sleeper anti-resonances, rail resonance and pin-pin resonance should be measured first with, for example, a hammer test, or with a model similar to that presented above. Any frequency in the first column of Table 2 may be related to squats. The sleeper anti-resonance and pin-pin resonance are also related to the formation of corrugation.[26] Thus, squat detection on corrugated track using only these two frequencies may be problematic, particularly for light squats with low ABA magnitude. In this case, the frequencies near 1530 and 1900 Hz can be used for the detection of light squats.

Conclusions

In this paper, the influences of different parameters on the signature tunes of squats were investigated. The ABA was found to be significantly influenced by the train speed. To eliminate the influence of the train speed, the measurements should be performed at nearly constant speed, and a mapping between the ABA measurements and speed is necessary when the measurements cannot be performed at a constant speed. The mapping relation between ABA and the train speed for one squat was presented. The relation between the train speed and ABA can be further investigated by simulations of defects of different severity. Additionally, one of the characteristic ABA frequencies at squats was found to be dependent on the position of the squat relative to the sleeper.

The relationship between the signature tunes of the squats and the track parameters was investigated. The signature tunes of squats were found to be the natural frequencies of the track: the sleeper anti-resonance, rail resonances and pin-pin resonance of the track. The signature tunes of squats may vary for different tracks because they are the natural frequencies of the track. The sleeper anti-resonance and pin-pin resonances are also related to corrugation. Therefore, higher-frequency components (i.e. 1000 and 2000 Hz) must be used for the detection of light squats on corrugated track. The development of more generic relations (mappings) and the inclusion of this information in an automatic squat detection system should be investigated in future research.

Funding

This research is supported by the Dutch Technology Foundation STW, which is part of the Netherlands Organisation for Scientific Research (NWO), and is partly funded by the Ministry of Economic Affairs. This work was supported by the Dutch railway infrastructure manager ProRail.

Acknowledgements

The authors would like to thank the anonymous reviewers for their valuable comments and suggestions.

References

1. International Union of Railways. *Rail defects*. Fourth ed. Paris, France: International Union of Railways, 2002.
2. RailTrack UK. *The blue book of rail damage*. London, UK: RailTrack, 2001.
3. Clayton P and Allery MBP. Metallurgical aspects of surface damage problems in rails. *Can Metall Q* 1982; 21(1): 31–46.
4. Frederick CO. International conference on rail quality and maintenance for modern railway operation delft, June 1992. In: Kalker JJ, Cannon DF and Orringer O (eds) *Rail Quality and Maintenance for Modern Railway Operation Book*. Netherlands: Springer, pp.3–14, 2003.
5. Sunaga Y, Sano I and Ide T. A practical use of axlebox acceleration to control the short wave track irregularities. *Railway Tech Res Inst, Q Reports* 1997; 38(4): 176–181.
6. Weston P, Ling C, Roberts C, et al. Monitoring vertical track irregularity from in-service railway vehicles. *Proc IMechE, Part F: J Rail Rapid Transit* 2007; 221(1): 75–88.
7. Bocciolone M, Caprioli A, Cigada A and Collina A. A measurement system for quick rail inspection and effective track maintenance strategy. *Mech Syst Signal Process* 2007; 21(3): 1242–1254.
8. Remennikov AM and Kaewunruen S. A review of loading conditions for railway track structures due to train and track vertical interaction. *Struct Control Health Monitor* 2008; 15(2): 207–234.
9. Li Z, Molodova M and Dollevoet R. Detectability of isolated short wave rail surface defects by way of axle box acceleration. In: *The 21st international symposium on dynamics of vehicles on roads and tracks* (eds Berg M and Trigell AS), Stockholm, Sweden, 17–21 August 2009, pp.1–11, 45. Sweden: KTH.
10. Molodova M, Li Z and Dollevoet R. Axle box acceleration: measurement and simulation for detection of short track defects. *Wear* 2011; 271(1): 349–356.
11. Molodova M, Li Z, Núñez A and Dollevoet RPBJ. Signature tunes of squats. *Struct Health Monit*, under review.
12. Molodova M. *Detection of early squats by axle box acceleration*. PhD Thesis, Delft University of Technology, The Netherlands, 2013.
13. Spannar J. A new approach of assessing rail roughness. In: *The fourth IET international conference on railway condition monitoring* (ed Roberts C), Derby, UK, 18–20 June 2008, pp.80–85. England: The Institution of Engineering and Technology.
14. Li Z, Zhao X, Esveld C, et al. An investigation into the causes of squats—correlation analysis and numerical modeling. *Wear* 2008; 265(9): 1349–1355.
15. Zhao X, Li Z and Liu J. Wheel-rail impact and the dynamic forces at discrete supports of rails in the presence of singular rail surface defects. *Proc IMechE, Part F: J Rail Rapid Transit* 2011; 226(2): 124–139.
16. PREN 13674-1: 2009. Railway applications – track – rail – part 1: Vignole railway rails 46 kg/m and above.
17. Hiensch M, Nielsen JCO and Verheijen E. Rail corrugation in The Netherlands—measurements and simulations. *Wear* 2002; 253(1): 140–149.
18. Li Z, Dollevoet R, Molodova M and Zhao X. Squat growth—some observations and the validation of numerical predictions. *Wear* 2011; 271(1–2): 148–157.
19. Li Z, Molodova M, Zhao X and Dollevoet R. Squat treatment by way of minimum action based on early detection to reduce life cycle costs. In: *The 2010 joint rail conference* (ed Barkan C), Urbana-Champaign, IL, 27–29 April 2010, pp.305–312. New York: American Society of Mechanical Engineers.
20. De Man AP. *DYNATRACK: A survey of dynamic railway track properties and their quality*. PhD Thesis, Delft University of Technology, The Netherlands, 2002.
21. Knothe K. Rail vibrations in the high frequency range. *J Sound Vib* 1994; 169(1): 111–123.
22. De Man AP. Pin-pin resonance as a reference in determining ballasted railway track vibration behaviour. *Heron* 2000; 45(1): 35–51.
23. Grassie SL, Gregory RW, Harrison D and Johnson KL. The dynamic response of railway track to high frequency vertical excitation. *J Mech Engng Sci* 1982; 24(2): 77–90.
24. Fenander Å. Frequency dependent stiffness and damping of railpads. *Proc IMechE, Part F: J Rail Rapid Transit* 1997; 211(1): 51–62.
25. Iwnicki S. *Handbook of railway vehicle dynamics*. Boca Raton, FL: CRC/Taylor & Francis, 2006.
26. Thompson D. *Railway noise and vibration: mechanisms, modelling and means of control*. Oxford, UK: Elsevier, 2009.